AC 2012-5021: PRECISION MEASUREMENT METHOD OF MISALIGNMENT, CRACKS, CONTOURS, AND GAPS IN AEROSPACE INDUSTRY

Dr. Devdas Shetty, University of Hartford

Professor of Mechanical Engineering and Dean of Research at the University of Hartford. Has published more than 200 papers and conference presentations and three text books.

The field of expertise of Dr. Shetty involves (1) Mechatronics System Desgn, (2) Innovative Product Design, (3) Laser Instrumentation, (4) Laser material processing, (5) Unmanned Aerial Systems, (6) Guided Projectiles, (7) Rehab System for Gait and Walking without fall, (8) Engineering education and (9) ABET accreditation.

Mr. Claudio Campana, University of Hartford

Claudio Campana is a Research Engineer at the Engineering Applications Center and Adjunct Professor of mechanical engineering in the College of Engineering Technology and Architecture at the University of Hartford, West Hartford, Conn. He holds a master's of engineering degree in mechanical engineering from the University of Hartford and a bachelor's of science degree in mechanical engineering from Boston University. His areas of research include computer-aided design and manufacturing, online inspection/supervision of manufacturing process, and mechatronics design and instrumentation.

Precision Measurement Method of Misalignment, Cracks, Contours and Gaps in Aerospace Industry

Abstract

Precise measurement of surface defects is of critical importance in parts manufactured for the aerospace industry. The measurements of different characteristics of the testing samples are presented in this paper. They are measurement of (i) micro scratches, cracks, (ii) contours and (iii) gaps.

The instrumentation setup for the measurement of the above parameters includes laser source, collimators, imaging and vision acquisition system, three axis (xyz) stage, graphical programming and computerized image analyzer. For measurement of the major geometrical dimensions of scratches and cracks a low power (2mW) Helium-Neon (HeNe) laser source has been used. Due to relatively high wavelength of the red photons irradiated from the HeNe laser source, the incident laser beam possesses a very high level of reflectivity and negligible penetration.

The experiments listed in this paper explore unique optical methods using a line laser. The advantage for using this type of laser is that it generates low energy red photons having about two to three electron-volt energy and possessing perfect reflectivity. The low energy photons have negligible low penetration. The paper explains a methodology for non-contact measurement of radius of curvature on the finished surface of manufactured parts. In addition, a hybrid approach consisting of laser based triangulation, photogrammetry and edge detection techniques has been investigated to measure inner surfaces of parts that have limited access, especially where human presence is impossible. The system is capable of detecting and measuring misalignments, gaps, inclinations as well as surface variations such as cracks and dents. The system employs the accuracy and speed of measurement of triangulation systems and combines these with the mobility and cost effectiveness of photogrammetry and edge detection techniques. In addition to gap and alignment offset inspections, and the instrument enables angle measurements, surface texture examinations and other inspections needed to be done inside assemblies with narrow openings, with its compact body. This topical area provides an ongoing thesis topic for graduate engineering students at the masters level.

Introduction

Non-contact methods are generally based on projecting energy waves to the surface and capturing the reflected or transmitted energy. Computer Tomography, Microwave Radars and Ultrasonic Waves are non-optical methods that are very common in measurement and inspection. Computer tomography is useful to examine internal cavities that cannot be seen from outside, on the other hand, accuracy with these systems is dependable on material densities that may be a problem for different types of materials. Microwave and ultrasonic methods are reflection based methods that typically measure the distance by calculating the time between creation of a pulse of microwave energy or sound and detecting the reflected waves. These detectors are inexpensive, but they are not very accurate in short distances. Triangulation, holography, active depth from defocus and moiré interferometry are some of the optical non-contact active shape acquisition methods. Unlike the passive and non optical approaches, active optical rangefinders can capture accurate readings in a very short time. Also they are less expensive and safer than industrial computer tomography methods. Highly accurate range detecting can be done with a fraction of light wavelength over micro fields. Active depth from focus (DFF) method is based on measuring the focusing distance between in-focus and blurred images. While passive DFF methods need surface textures, active DFF's have reflected grid patterns. Previous works show that, these methods have a moderate accuracy [1]. Active stereography method consists of two or more cameras capturing a part of the object and finding differences of two images, captured from different angles. Several techniques are available for three dimensional acquiring of objects. The methods have a variety of capturing hardware, accuracy and cost [2]. Computed Axial Tomography (CAT) is an expensive method in which a detailed surface data of an object can be obtained. Three dimensional spatial sampling is a less expensive alternative which is based on video streams, or determining silhouettes or some space carving techniques. The most important advantage

of laser scanning is the non-contact processing which allows fast acquisition of point coordinates from the surface. With the non-contact processing, fragile parts can be measured and surfaces of fragile objects can be captured.

Current Measurement Tools

There are many commercially available instruments which are capable of measuring the radius of curvature for manufactured parts. Such instruments include gap-guns, spherometers, profiloscopes, and capacitance sensors. These are limited in terms of range of measurement and access to the features to be measured [1]. In producing purpose-built instrumentation for surface measurement of specific components some form of improvement may be made over commercially available instrumentation. Aerospace companies continuously seek quality control methods which are accurate and robust. Many precision components, such as root-attachment areas of turbine blades, include intricate shapes and features having a small radius of curvature. Each of the above mentioned methods of measurement have disadvantages to assessing the surface features of such components.

Gap-guns are a hand-held, wireless form of laser gauge which may be used to assess surface features such as gap depth and width, step height, hole-diameter, and radius of curvature. Measurements are made through laser triangulation [2]. As these devices are hand-held, great care must be used in aligning the gap-gun head with the feature to be measured, with measurements becoming increasingly difficult to make across intricate surface geometry. The gap-gun laser must have direct access to features of interest, excluding this type of device from use as a measurement tool for components with features which are obscured by other surface geometry.

Spherometers are a specific type of micrometer which may be used to measure the curvature of a surface. When used in this case, three support legs and one measurement leg of the instrument must all contact the surface containing the curvature to be measured. A difference in vertical displacement between the support and measurement legs is used to deduce the radius of curvature of the surface [3]. The requirement that the support legs make contact with the curved surface precludes this type of instrument from use in the measurement of very small radii.

Templates may be used to determine deviation from design of manufactured parts containing intricate geometry and small radii. For this type of component assessment high-precision templates must be produced for each component to be inspected. Apart from the cost associated with producing templates for each component to be inspected, the primary disadvantage of this type of assessment is the high possibility of damage to the surface of the components being examined as a result of contact between the template and component.

Profiloscopes are instruments which were traditionally used in measuring the surface profile and radius of curvature of objects. Some industries still apply this technique, with updated instrumentation, in the assessment of surface features today. Profiloscopes produce a diffrimoscopic projection or image of a component to be assessed at a known magnification and measurements are read across the projection. These measurements are then scaled to actual values using the known magnification level [4]. High levels of magnification are required for the measurement of small radii, multiplying error associated with the measurements. Improvements may be made over this method through process automation.

Capacitance sensors may also be used to determine radius of curvature. These instruments measure changes in capacitance between the sensor and a conductive sample. As the gap between the sensor and sample changes, such as when the sensor is scanned at a given height across a curved surface, a change in capacitance between the two is recorded. Any surface curvature present in the sample may be calculated by mapping the change in distance between the sensor and sample as a function of location across the sample surface. The relationship between the size of the instrument sensing area and the area to be measured is critical to the performance and accuracy of these devices. It is typically required that the area to be measured be 30% larger than the sensing area of the capacitance sensor [5]. This requirement limits the viability of this type of sensor being an appropriate choice for the measurement of very small radii.

Major advancements have occurred in three dimensional vision systems. Three dimensional vision systems consist of two light sources projecting two slit images perpendicular to each other, and an image sensor which detects the intersection of the lines via a rotating mirror system [6]. This type of system measures displacement from the surface

as a one dimensional rangefinder. The system captures minimum and maximum signal levels as compared with the standard surface data. This type of system is not capable of inclination measurements. Contour Measurement Using Time-Based Triangulation Methods' may be used to measure surface contours via triangulation [7]. This type of system is capable of detecting edges of reflective metal surfaces, excluding its use for measuring surface contours of non-reflective materials such as coated ceramic or most plastics. Three Dimensional Vision System consists of two light sources projecting two slit images perpendicular to each other, and an image sensor detecting the intersection of lines with a rotating mirror system [3][8]. This system can measure the distance from the surface only as a one dimensional rangefinder, at a time. The system is capable of detecting the surface with the help of a rotating mirror and capture highest and lowest signal levels, which can be compared with the standard surface data. The system is also not capable of inclination measurements. Contour Measurement Using Time-Based Triangulation Methods describes a non-contact methodology which can measure surface contour by using triangulation [4]. The system is capable of edge detection of reflective metal surfaces. It uses the reflection principle, which cannot be used in non-reflective materials such as coated ceramic or most plastics. Speckle Reduction Track Filter Apparatus for Optical Inspection of Patterned Substrates projects two patterned image maps to a surface and detect to macro moiré effects on the surface [5]. As the system uses diffraction as a detection method, non diffractive material inspection is not possible with the apparatus. Non-Contact Precision Measurement System uses laser as a non contact component in its measurements [6]. The system depicts a good approach in measuring parts which are portable due to the rigid installment requirement of the system. The system is not flexible enough to enter a cylindrical tank, or a jet engine. Method for the Contact-Free Measurement of the Distance of an Object According to the Principle of Laser Triangulation is a laser triangulation based system which can precisely measure a point XY coordinates [7]. It is hard to measure inclinations with this setup due to its point based capturing nature.

Development of Methodology for Inspection

Triangulation is most widely used optical approach in range finding. It is based on emitting light and capturing the reflectance with a sensor. The sensor observes the reflected stripe which has geometry similar to the surface and different from the line. Measuring the difference is the base of triangulation methods. This can be seen in Figure 1. In Fig. 1(a), a surface is illuminated by a narrow laser beam, and the linear sensor captures the reflection from that surface. In Fig. 1(b), a laser line, can also be called as laser sheet, is generated by the cylindrical lens and projected to the surface. In general, the needed inspections and measurements can be classified into alignment offsets in assemblies, gaps in assemblies, diameter changes, bumps, cracks and angle between surfaces.

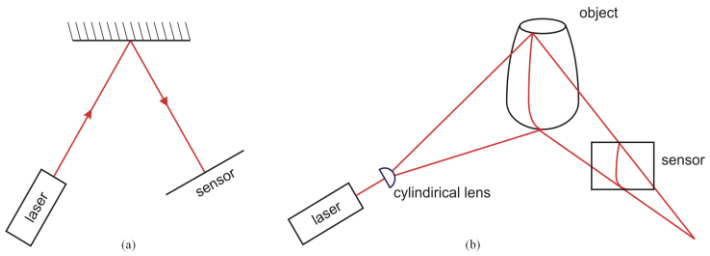

Figure 1. Triangulation

The proposed optical triangulation methodology in this paper is the basis to develop a new system that is compact, digital and adaptable. The simplest way to generate three-dimensional information from a scene is to do it one point at a time, using a method known as point triangulation. The working principle behind this method is based on simple trigonometry. Laser as a source, a digital camera, and the laser's spot on the surface form a triangle. Measurement of the distance between laser and the camera and the angle between the camera and laser projection allows easy determination of the distance between camera and the point on surface. This range gives the third dimension, and can be determined for every object point by scanning the laser beam across the surface. This method is very powerful technique and is used frequently for three-dimensional scanning because of its straightforwardness. The problem for

this type of system, though, is that it has a comparatively slow scanning speed. Digital output may have more than a quarter of a million points. The system can only record a fraction at a time, so total recording time is long. The three-dimensional output image, like a long exposure photograph of a moving object, can sometimes be blurred for all but the most motionless substances. This problem may be solved by a technique known as line scanning that is used frequently. Line triangulation or line scanning, is a simple extension of point triangulation method. In the line triangulation technique, the projected light is a line and an entire strip of the surface is scanned at a time. Required time to scan a surface is significantly less, but the computational algorithms are more complex for the line triangulation method.

Hardware and software used in the system are Edmund Optics High Performance Structured Light Laser Diode Module, Sony XCL-U1000 Black and White Digital Video Camera, Fujinon HF50HA-1B Lens & Hoya UV(0), NI IMAQ PCI/PXI-1428 High Quality Camera Link Image Acquisition Device, NI PXI-8105 2.0 GHz Dual-Core PXI Embedded Controller, Newport KPX118 and KPX124 Plano-Convex Lenses, Newport KBX082 Double-Convex Lens, Edmund Optics C54-184 Interchangeable projection, Newport 10D10 ER.2 Metallic Mirror, Newport RG-22-2 RG Series Breadboard, Parker MX80M Miniature Stage, National Instruments Vision software

Experimental System

The system can be analyzed in two main parts as the Laser Projection Element, and the Image Capture Part.
The Laser Projection Element (LPE) basically consists of a HeNe laser source, planoconvex lenses, a line generator projection head and a metallic mirror. The laser source produces a red laser in 670 nm which has an output of 3 mm beam. Since the divergence is negligible within our measurement limits, the beam will be considered as quasi parallel. After two inches from the source that the beam is emitted, a planoconvex glass element which has a 500 mm effective focal length is pre-focusing the beam. The desired focus plane is 9 inches perpendicular from the laser line. To produce a perfect thin line at that length, another planoconvex lens which has a 1000 mm focal length is used to focus the beam to 16 inches distance from the laser source. That setup enables the 9 inches target measurement. The effects of the lenses on the beam can be seen in Fig. 2.

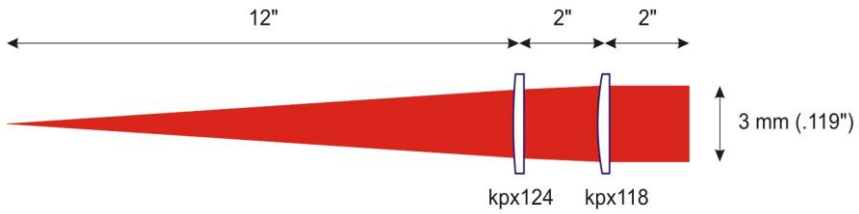

Figure 2. Laser Beam Profile

The lenses are utilized to produce a very thin line on the target. The projection head generates a line at a distance of 2 inches for the above set up. . The projection head in the system has a divergence of 30 degrees. Using the following equation, the value of X is found to be 122.5mm.

$$X = 2L * \tan(\alpha/2) \quad (1)$$
$$X = 4.823 \text{ inches} = 122.5 \text{ mm.}$$

The final design for LPE is shown below in Fig. 3. As can be seen from the figure, current LPE is designed to measure 9 inches distance from the mirror. For a different length, the middle optical system should be optimized. Image Capture Part (ICP) basically consists of an optical system, high resolution digital camera, image acquisition card, and a PC and machine vision software.

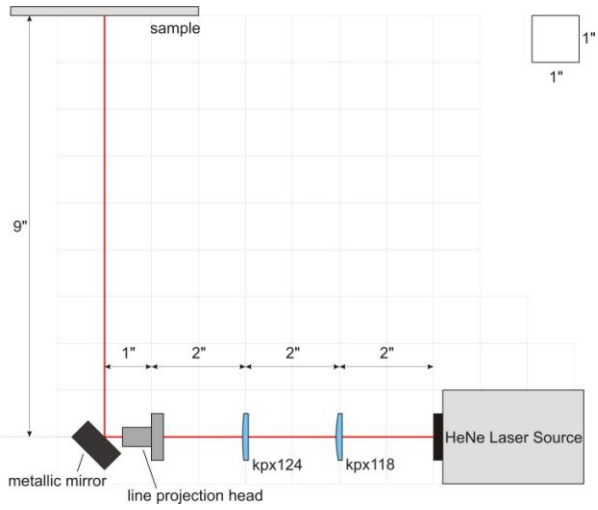

Figure 3. LPE Overview

The camera is positioned parallel and close to the laser source. Location for the camera is designed to make a compact and flexible body. For a greater magnification and shorter minimum focal distance, a double convex glass element is used after the mirror. For an X inches measurement setup, the mirror angle can be found as follows.

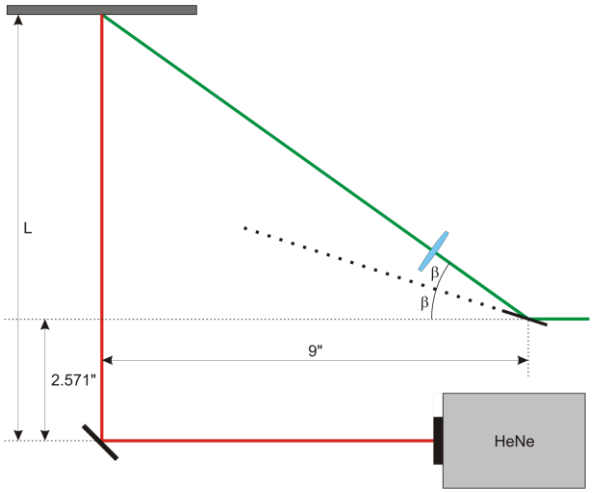

Figure 4. Mirror angle equation

$$\tan(2\beta) = (L - 2.571) / 9$$
$$\beta = 0.5 \arctan[(L - 2.571) / 9] \quad (2)$$

As the mirror angle β is known, the double convex lens should be positioned with a (90 - 2β) angle with the horizontal axis. A mechanism can be designed for the mirror and lens with a 2:1 rotation ratio. Note that the L is different from the distance of the generated line used in Equation (1). Finally the angle of view is shown below for the 9" target setup in Fig. 5. Red line shows the laser and green lines show the angle of view. The final area detected from the sample is 1" x 1.33". The measurements will be described in the following part. Final design can be seen below in Fig. 6.

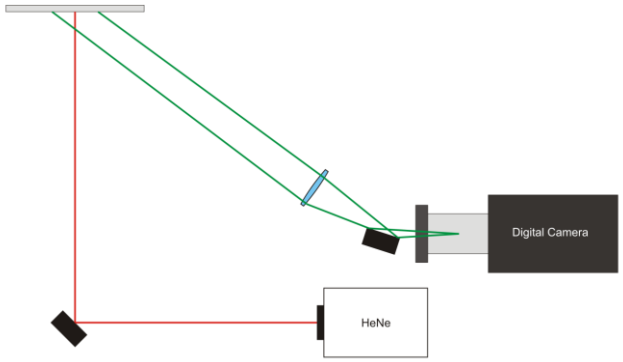

Figure 5. View Angle

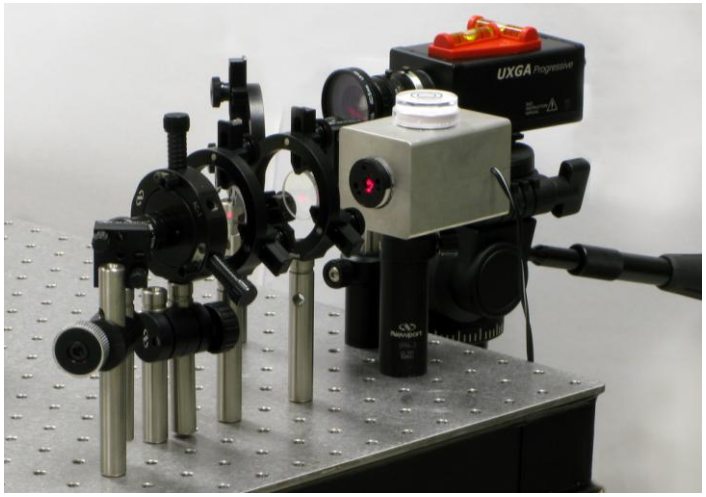

Figure 6. System Overview

Misalignment Measurements

The desired accuracy and precision levels and the used equipments created new specifications for the measurements. For a lower tolerance, a smaller view was needed, and that meant higher grade optics and a much more pixel data. At that point, a 1" x 1.33" viewing area has been selected. For a 1600 x 1200 pixels, the selection provides 8.33×10^{-4} inches per pixel resolution. That will be the base for measurements. A higher magnification constant could be selected for a higher inches per pixel resolution, but it would cause a view of a very small area. The selected resolution and magnification constants are perfectly fit to the sample design. Calibration sample is designed to provide three different heights, made from white plastic stripes with thicknesses of 300 µm, 500 µm and 1000 µm. With 100 µm double sided scotch tape, heights of the stripes became 400, 600 and 1100 microns. Current devices are generally designed to determine dimensions for metallic materials. For a non metal, laser reflection cannot be detected with a conventional density sensor. The designed sample will give a result that not any other conventional method can give.

Initially, HeNe laser source is projecting the laser through the lenses to the line generator. After HeNe laser line is generated through the projection head, it hits the sample surface. With an angled view from the camera, height of the plastic stripes can be found. A simulated laser reflection profile can be seen in Fig. 7. Laser line makes two different reflections from different heights. Difference of the two lines captured will be detected with machine vision software, and positions will be read. After finding the points, pixel position data will be converted to pixel length data. Then

this length will be used to find Calibration Factor (CF) that will be used in real world examples. The main approach is capturing different lines from another angle. The camera is located to capture the different lines. System layout can be seen in Fig. 8. NI Vision Assistant is used for capturing and processing images from the sample. The program is working bi-wired with the Labview. Any changes in the acquired image or any real-time captured scenes will directly change the output from Labview. As a result, an interactive, on-line capturing and measuring are possible via designed system.

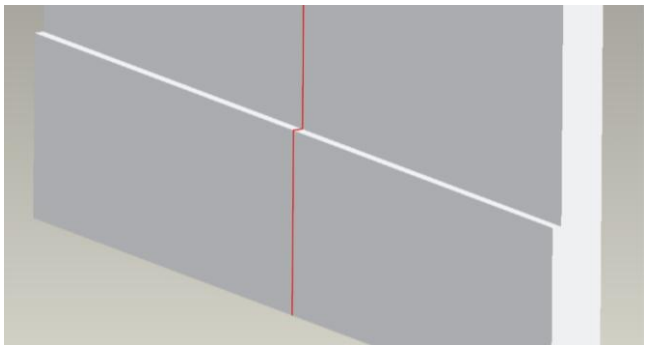

Figure 7. Simulated Laser Line

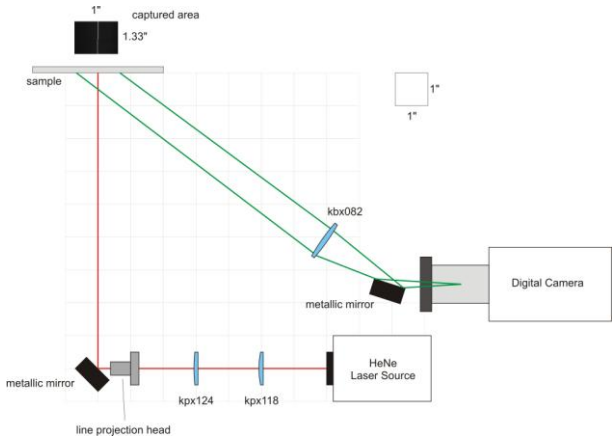

Figure 8. System Layout

NI Vision Assistant has a lot of features like line detectors, edge detectors, calipers and histogram tools for machine vision applications. The measured area shows the laser line, reflected from two different surfaces. For that point, it should be noted that the captured laser lines should be in the middle of the acquired scene to minimize perspective errors. The reflecting angle, viewing mirror and biconvex lens position and angles are designed to make measurements from the middle part of the image. For the specifications determined, 14% of the image is used. As can be seen from Fig. 9, there are some spherical and perspective errors, but within the area selected, all aberrations are negligible. From the millimetric scaled target shown, thickness of the laser line can be measured approximately 0.4 mm. In the real testing, the middle points of the laser profiles will be used to generate line. Perspective error for the specified area and viewpoint aberration angles for 9 inches target are shown below in Fig. 10.

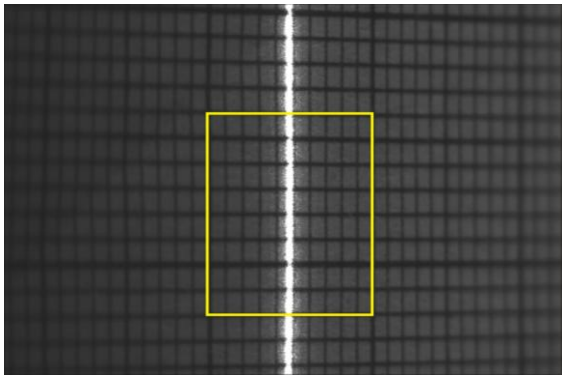

Figure 9. Effective Measurement Area

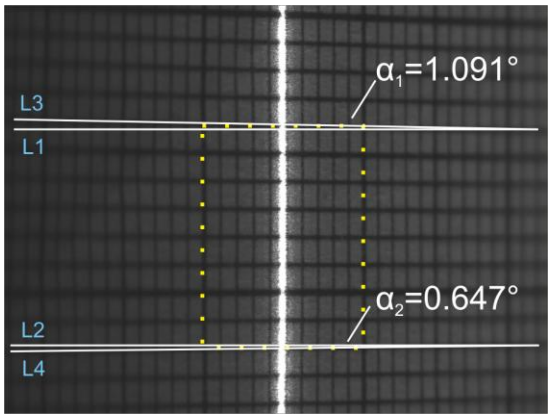

Figure 10. Perspective errors.

As can be seen from Fig. 10, L1 and L2 are parallel to each other. L3 and L4 are the real vertical lines. Angles between them are $\alpha_1 = 1.091°$ and $\alpha_2 = 0.647°$, so the total perspective error is $\alpha_{TOTAL} = \alpha_1 + \alpha_2 = 1.837°$. For the measurement area, perspective errors are in the limits.

Calibration Factor

For different measurement lengths, mirror and magnification lens angles should be changed. Also view angles of camera should be changed with a new setup. To make correct measurements in different measurement limits, the system needs to be calibrated. A calibration coefficient should be determined for a measurement distance. This constant will be called Calibration Factor. This factor is basically a unit dimensional magnitude for each pixel detected. So the calibration factor can be defined in inches per pixel or microns per pixel. To determine calibration factor for a system, a known target should be used. As the dimensions of the sample described above are known, it will be used as calibration target. Calibration Function can be defined as,

$$CF = h / p \quad (3)$$

where h = real height of the alignment offset, p = pixel count.

The initial setup is designed to measure depth in 9” distance. From Equation (4), β can be found as,

$$\beta = 0.5 \arctan [(L - 2.571) / 9] \quad (4)$$
$$\beta = 17.77°$$

The distance between biconvex lens and mirror is 2.458” that can also be found from sinus function. After the calculations, the view system setup should be positioned as shown in Fig. 11.

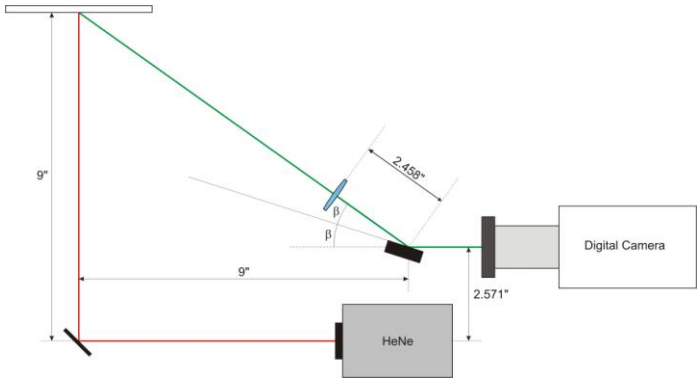

Figure 11. Final Setup

After positioning the elements for the Image Capture Part, the system becomes ready for measurements. The method for measurements is first measuring the target that is known and finding the Calibration Factor for the setup, and then making measurements with that factor.

Calibration for Height and Misalignment

First of all, the 1100 microns height is selected. Once the image is captured and saved to the browser, it can be opened with process image toolbox. The “test and measurement” option, and then the length option are selected. This feature measures the line drawn between two specified points. At first, the end of the first line, then beginning of the second line is selected. This will record the data to a spreadsheet file. To get a better result in terms of precision and accuracy, 50 different measurements are taken. After calculating the mean of the measurements in pixels, the Calibration Factor will be defined. The measurements and a 10 times zoomed image is shown below in Fig. 12

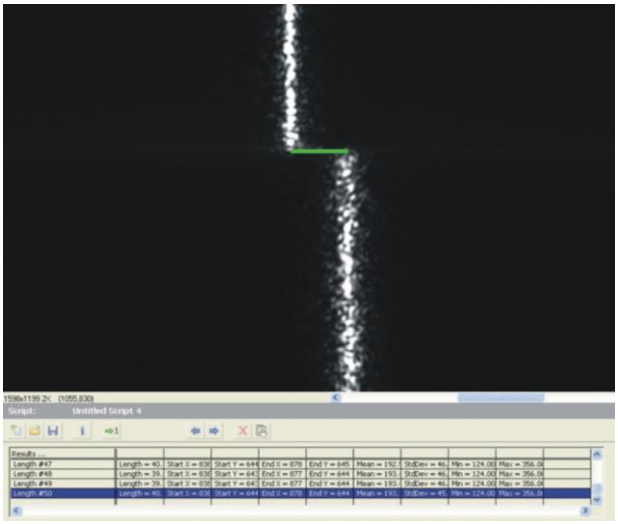

Figure 12. Measurement line and results.

Note that the green measurement line is thickened for a better vision and print. The results are shown at the bottom of the figure. The results are then copied to Microsoft Excel, to find mean value and Calibration Factor. Mean for the 50 measurements for the first setup is 40.8603112 pixels. That should equal to 1100 microns, so the Calibration Factor can be found from,

40.8603112 pixels = 1100 microns
CF = (1100/40.8603112) = 26.92098929 µm/pix

Secondly, 600 µm offset is measured with the same method used in the first experiment. For this measurement, tilting the camera upwards, of changing the angle of laser reflecting mirror may change the CF. Consequently, a vertical driven micro stage is used. By using this way, the laser line, and the camera view remained the same. The mean and CF are found as,

Mean = 22.2862592 pixels
CF = 26.92241864 µm/pix.

As can be seen clearly, the system measures consistently, as the CF's are almost same. The measured area for 600 microns can be seen below.

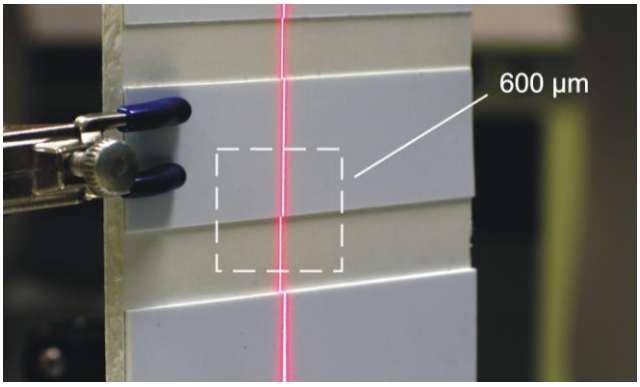

Figure 13. 600 microns offset

Finally, 400 microns target is measured to ensure the consistence of Calibration Factor. After 50 different measurements are done, the results are imported to Microsoft Excel. The mean, Calibration Factor are found as,

Mean = 14.826912 pixels
CF = 26.9779705 µm/pix.

The results show that the system is consistent, and measures correctly within the limits. As a result, calibration for height measurement has been done, and CF's are found as,

CF (1100) = 26.92098929 µm/pix.
CF (600) = 26.92241864 µm/pix.
CF (400) = 26.97797050 µm/pix.

These similar numbers show the consistency of the system. Because the most accurate reading is the biggest distance reading, the CF for 1100 microns is used for any measurements with the 9 inches setup. By selecting CF as CF (1100), the reading errors can be found as,

h = read pixels x CF (1100) = 599.968145 µm
% Error = -0.0053% (for the 2nd set)
% Error = -0.21% (for the 3rd set)

From the calculations above, it can be seen that, the errors are very low and mostly higher when the measured distance is extremely small. For the specifications mentioned, the errors are in the limits. As a result of the first three experiments, it can be identified that the system can easily inspect the assembly parts whether they are perfectly aligned or not. And also the difference between the two non-perfectly aligned parts can be measured. For next, the same calibration sample can be used for another measurement distance. To find new CF's, just needed is the change of the viewing angle and accordingly the angle and position of the magnification lens.

Misalignment Measurement using Aluminum Sample

Desired alignment measurements are for aerospace industry which mostly aluminum and titanium materials are used with special coatings. For testing the designed systems accuracy, a non-perfectly aligned aluminum prototype is made. The part mainly consists of two aluminum L shaped beam combined with clamps with virtually no gap but aligned with a distance. The reason that aluminum is used is to show that the system can measure different types of materials instead of white solid coatings. The prepared aluminum assembly is shown in Fig. 14.

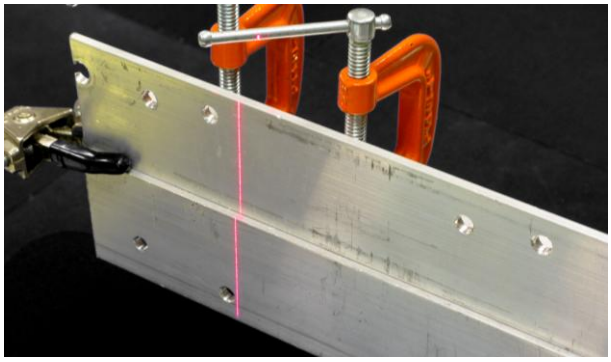

Figure 14. Aluminum Sample

The part is both illuminated with environmental light and laser. While the measurement may be needed in the inner surfaces of a part like turbines, the measurements are done with the environmental lights turned off. The sample is positioned to 9" distance that we know the Calibration Factor. And after the lights are off, the image is captured with NI Vision Assistant as shown below in Fig. 15.

Figure 15. Acquired Image from Aluminum Sample

For this test, instead of line determination, a point measurement method is used. With this module, points from each edge are selected several times, and the mean positions are found. After that, the horizontal difference is calculated from the pixel data, and the final pixels are multiplied with the CF, as found before. By calculating mean with Microsoft Excel, the two positions are found as, *X1=772.833*and *X2=914.13.* So, the distance is,

X2–X1=141.3 pixels.

And by multiplying this with CF, which is actually CF (1100) found before, the exact offset can be found as,

h=141.3x26.92098929=3803.9358 μm.

The final result is then measured with a micrometer, and the same results are taken.

Gap Measurement

In some situations, like an unwanted gap because of a non perfect surface of assembled parts, the dimension of the gap should be determined and measured. With the following two sets, measurement of the gap between two parts is aimed. In this experiment, a calibration sample will be produced to find a Gap Calibration Function, which is different from the CF found before. The difference is, while the CF is used to find horizontal distances, GCF will be used to measure vertical distances. The measurements will be done within the 9 inches length, as done before. After finding a GCF from the sample, a real world example will be shown. In the 6th experiment, two aluminum parts will be assembled with a metallic ruler between them. So there will be a gap between two parts. As a calibration sample, two 5 mm cardboards with a 0.175 inches gap between them are attached to a bigger white cardboard surface. As the 9 inches measurement length is selected, not any angles will be changed. The prepared sample is shown in Fig. 16. As can be seen from the figure, the continuous laser line is split in the gap area. To measure that distance, beginning and the end points of the gap will be found, and the vertical distance between them will be determined in terms of pixels. After finding the pixel data, the GCF will be found. After positioning the gap calibration sample to the effective view area, the image is acquired as shown in Fig. 17.

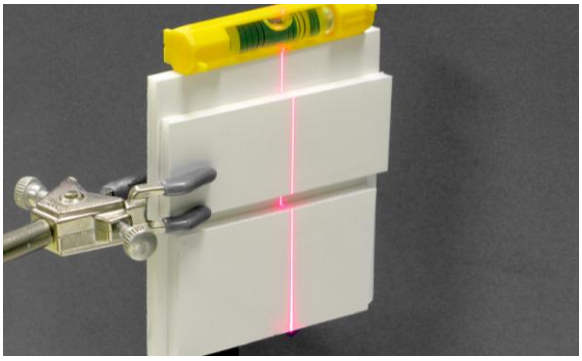

Figure 16. Gap Calibration Sample

Figure 17. Acquired Image

After capturing, the endpoints data of two lines reflecting from upper surfaces are read and pasted to Microsoft Excel. After the measurements, the vertical distance will be found. The mean values for Y positions for the beginning and the end of the gap are found as, *Y1=484.5* and *Y2=717.575*. So the vertical distance is, *d=Y2–Y1=233.025*

pixels. The distance should be 0.175 inches = 4445 µm. As a result, Gap Calibration Factor can be found as, *GCF=4445/233.025=19.0752 µm/pix.* With this coefficient, any gaps can be examined in the real world examples.
In this experiment, formerly described two aluminum parts are used. The parts are attached with a metallic ruler between them causing a gap that is actually the thickness of the ruler. The prepared sample is shown in Fig. 18. As seen, the parts are leveled in all measurements with a linear bubble level. Also it can be seen that the line discontinues in the gap area. After positioning the sample to the 9 inches distance, image is captured for point readings. The captured image is shown in Fig. 19. From NI Vision Assistant's measurement tools, position is selected, and the two edges are read with a set of 60 experiments. Means of the vertical points are calculated as,

Y1=600.133, Y2=654.8, d=54.667 pixels, L=1042.784 µm.

It is proved that the system can also measure gaps with a more precision than alignment measurements because of the smaller number of GCF than CF. While the alignment measurement system can measure 26 microns with the current setup, gap measurement system can measure 19 microns. From the captured images, it can be seen that the horizontal distances are for alignment offsets, and the vertical ones are for gaps. In the next experiment set, both will be inspected in one system.

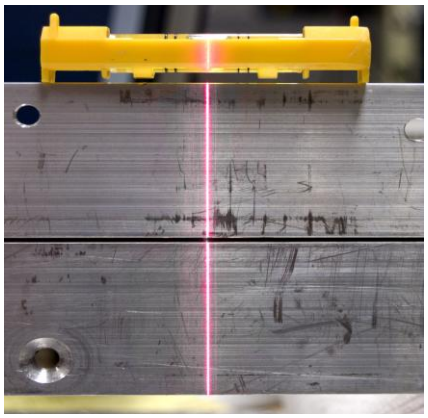

Figure 18. Aluminum Sample

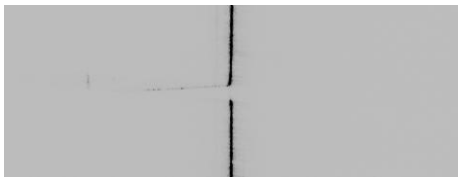

Figure 19. Captured Image

Measurement using Depth of Field

In the first example sets, and in the methodology section, it is mentioned that the system can measure pixel data, and with a calibration constant that is found by measuring calibration samples, system can measure the exact dimensions of the depth of alignment offsets and height of the gaps. But for each measuring distance, a new calibration constant is needed. In this experiment, regardless of the camera viewing angles, depth of field for different measurement distances will be found. First the millimetric scaled target is placed to 8 inches distance by using a micrometric driven horizontal stage. Then the camera view angle is determined for the setup from the equation,

$$\beta = 0.5 \arctan [(L - 2.571) / 9] \quad (5)$$
$$\beta = 0.5 \arctan [(8 - 2.571) / 9] = 15.55°$$

While the image is being captured in the effective area, by using the micrometer stage, target is moved forward and backward. When the laser line hits both the borders of the effective area, distance is read from the scale. For the 8 inches target, the limits are found as 30.95 mm and 21.14 mm. So the distance between them is 9.81 mm. After the measurements for 8 inches, target is placed to 9 inches distance, and same measurement is done. The limits are found as 36.10 mm and 25.15 mm. At third, for the 10 inches distance, limits are found as 34.83 mm and 22.50 mm. And finally for the 11 inches measuring distance, limits are found as 36.26 mm and 22.50 mm. So the distances between them are the depth of fields, as will be called DOF's.

For 8" = 203.2 mm, DOF = 30.95 – 21.14 = 9.81 mm
For 9" = 228.6 mm, DOF = 36.10 – 25.15 = 10.95 mm
For 10" = 254 mm, DOF = 34.93 – 22.50 = 12.33 mm
For 11" = 279.4mm, DOF = 36.26 – 22.50 = 13.76 mm

As can be seen from Fig. 20, depth of field increases while the measuring distances increase. But more distance means less resolution. So a higher magnification lens should be used with far settings. For the magnification lens and the viewing setup, 9 inches is selected as a measurement distance

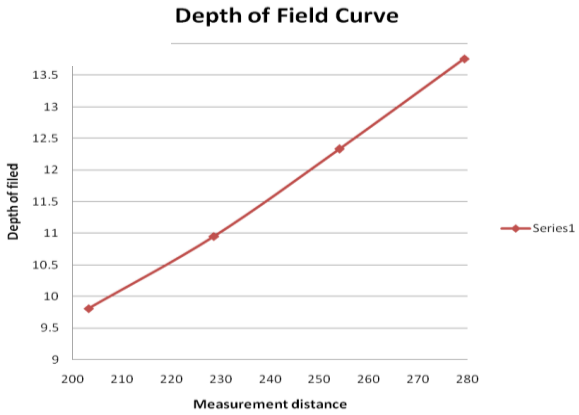

Figure 20. Depth of Field Curve

Discussion

Triangulation method is used as a base for the system. Although there are plenty of systems using triangulation for range measurement, they all have some disadvantages like big size and non-adaptability for the needs mentioned in the first section. In this paper, mainly two different types of inspections are done. While gaps are measured with the laser line discontinuity, the alignment issues are measured with the triangulation methodology in the same body. Alignment offsets that are not visible from front view are visible from an angled view. It can be seen in Fig. 21. The distances between the vertical lines are the depths of the offsets. When seeing from an angle, visual distances are different from the original distances. With the *Law of Sines*, the relationship can be defined easily. Basic description of the difference can be seen in Fig. 22.

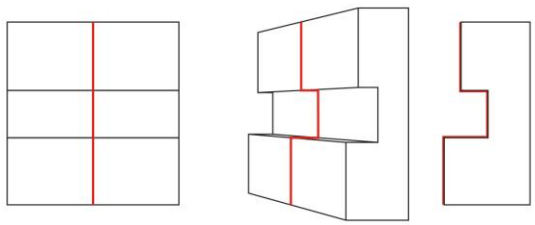

Figure 21. Alignment Offset

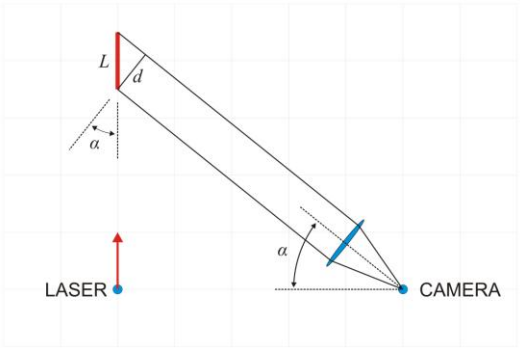

Figure 22. Distances in Triangulation Methodology

As can be seen from the figure, *d* is the viewed length, *L* is the original length and *α* is the camera angle. So the real length is found from,

$$L = d / \cos \alpha \quad (6)$$

In the first experiment sets, a misalignment issue was simulated. A sample with different heights was produced and measured. For consistency in dimensions, sample was measured 3 days, and another 4 days after it was produced. As the dimensions were the same, the sample was considered as calibration sample. Misalignment measurements were done in 9 inches perpendicular distance from the body. And the image were captured for 1100, 600 and 400 micron offsets for finding calibration factor. After finding the factor, any offset measurements were being possible. Image was captured and the horizontal distance between two lines was considered as the offset that has been calculated from pixel data x calibration factor equation. After the test, sample was measured with digital calipers, and same result was obtained.

In the subsequent experiment sets, gap between two assembly parts was simulated. A sample from cardboard with a gap was prepared with known dimensions and measured with calipers. Upon getting same results, the sample was considered a gap calibration sample and put in 9 inches measuring distance. The image was captured and pixel data is converted to a μm/pix unit that was as well a gap calibration factor. After finding GCF, a real world example was simulated again with aluminum parts. After the image was obtained, the endpoints were positioned and the vertical distance was found as pixels. Finally results were found by multiplying the pixel data with GCF.

The last experiment with aluminum parts was measuring both alignment offset and gap in an assembly. As the same 9 inches setup was used, calibration factor and gap calibration factor did not change. After the image was captured, the vertical distance between two endpoints was multiplied by GCF and horizontal distance was by CF to find the distance of gap and the offset. The vertical and horizontal distances and their meanings can be seen in Fig. 23.

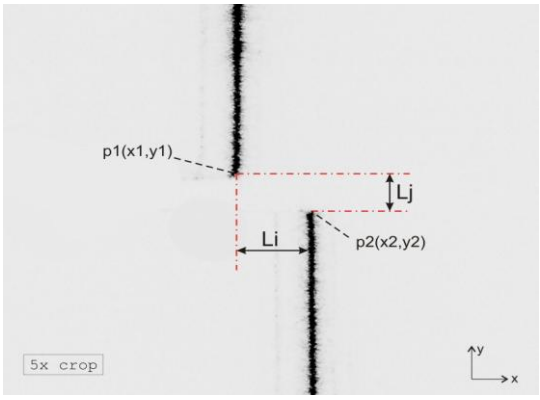

Figure 23. Captured Image

From the figure, two lines that are reflecting from two different surfaces can be seen. Endpoints are labeled as p1 and p2. From the machine inspection software, positions of two points are located as p1(x1, y1) and p2(x2, y2). Vertical distance between two endpoints is caused by a discontinuity. That may be a gap, a crack, hole or a cavity placed perpendicular to the line. So the Lj distance defines the measurement of gap, perpendicular distance of a crack, diameter of a hole, or any similar irregularity. By multiplying the distance with Gap Calibration Factor that is found for the same measuring distance, real distance can be found.

$$d = Ly = Lj \times GCF \quad (7)$$
$$d = (y2 - y1) \times GCF \quad (8)$$

Horizontal distance between two lines is caused by a height change in z direction that is perpendicular to surface plane. That change may be an offset in assembly, a bump or a diameter change inside a cylinder. Li distance expresses this offset, or height of the bump. Real magnitude can be found by multiplying the Li with Calibration Factor for the same measuring distance.

$$h = Lx = Li \times CF \quad (9)$$
$$h = (x2 - x1) \times CF \quad (10)$$

The results show that the system is capable of inspecting various cases and measure them.

Contour Measurement Experiments

The non-contact method of measurement of surface features proposed herein dictates that measurements are taken from an image of the feature of interest. A high-contrast image must be used in which the edge of the feature to be measured is clearly distinguishable from its surroundings. A line laser is projected across the feature to be measured and the sample is blocked from all other light sources. A calibration chart is held in front of the sample parallel to the image plane and an image is captured. From this image a relationship of pixels per unit length is determined.

Surface feature geometry is measured from the images using National Instruments Vision Assistant (NIVA) software. The original images are converted to 8-bit files and are imported into the NIVA program. Characteristics of the images such as contrast and sharpness may be adjusted. Once the edge of the feature to be measured is clearly distinguishable from its surroundings, an 'edge detection' tool is used to map data points across the feature to be measured. A second-order polynomial trend-line is fitted to the data points and Equation (11) is used to extrapolate the radius of curvature from the measured data. An image of a line laser projection across a cylinder is shown in Fig. 24.

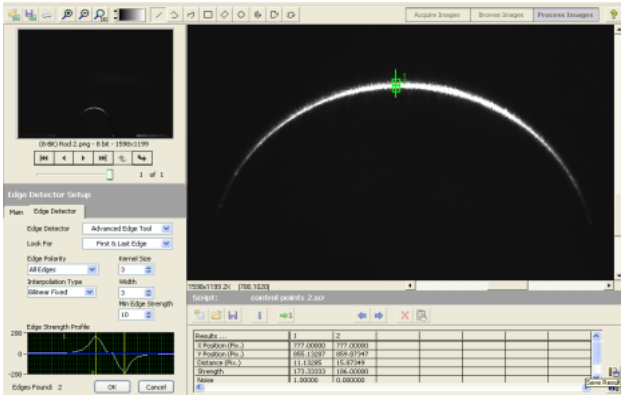

Figure 24. Feature Edge

$$R = \frac{\left[1 + \left(\frac{dy}{dx}\right)^2\right]^{\frac{3}{2}}}{\frac{d^2y}{dx^2}} \quad (11)$$

The test setup for the line laser method includes a line laser (1), sample (2), and a machine vision camera (3) at some elevation and angle to the sample as shown in Fig. 25.

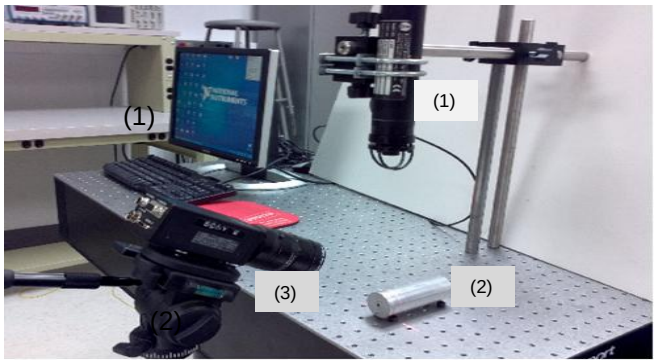

Figure 25. Detector Arrangement: Line Laser Method

A process map for the line laser method is shown in Fig. 26. A line laser is projected across the region of interest of the sample and a machine vision camera captures an image of the line laser projection across the sample. This image is manipulated and evaluated using National Instruments IMAQ Vision Assistant software. Image contrast and filter settings are adjusted to optimize the clarity of the line laser edges for measurement. An edge detection tool within the software is used to map data points along the upper and lower edges of the line laser projection. These control points are then adjusted to account for the angular displacement between the camera and sample and to provide a characteristic set of data points along the centroid of the line laser image. A second-order polynomial trend-line is then fitted to the data points and the radius of curvature of the trend-line is evaluated using Equation (11).

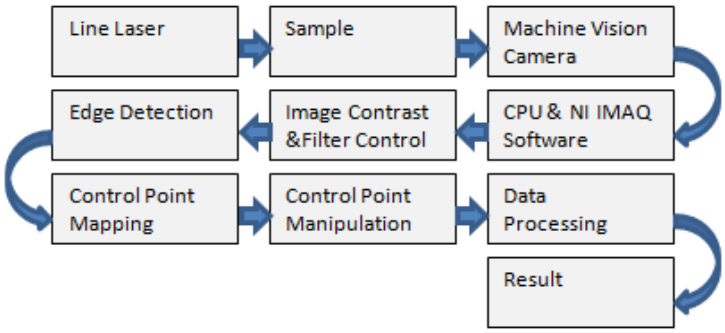

Figure 26. Process Map: Line Laser Method

Some amount of angular displacement between the image plane and measurement plane is required as images orthogonal to the measurement plane will not provide a direct view of the laser projection across the sample. Once an image is captured the 'edge detection' tool within the NIVA software is used to map data points across the lower and upper edges of the line laser, producing two y-values for each x-value. These y-values are then averaged in order to provide a single characteristic y-coordinate for each x-coordinate. An image containing a line laser projection across a cylinder with data points mapped across the lower and upper edges of the line laser is presented in Fig. 27.

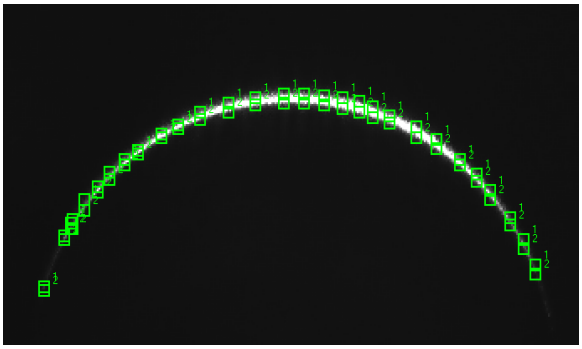

Figure 27. Data Points – Line Laser

The angular displacement between the image and measurement planes will tend to skew the image and data points in the y-direction, requiring that the y-values of all data points be multiplied by the cosine of the angle between the image and measurement planes.

Figure 28 presents the relationship between the image and measurement planes and outlines the need for manipulating the y-values of the data point coordinates. The image plane is perpendicular to the view axis of the camera. The plane through which the line laser is projected is defined as the measurement plane. Due to the angle between the two, the height of data-points as captured within the image plane must be mathematically manipulated to actual values.

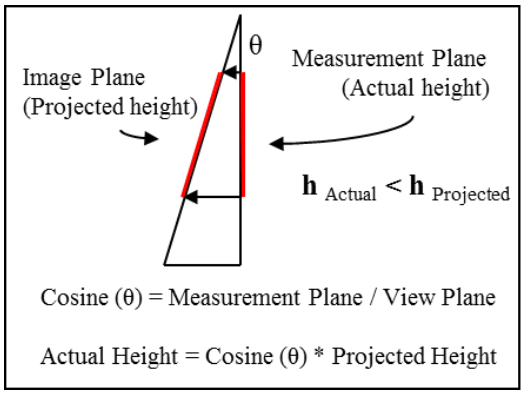

Figure 28. Image Projection Diagram

Industry specific samples for measurement were provided by aerospace industry engine manufacturer Pratt and Whitney Aircraft Company. These samples contain features which would be likely candidates for a precise, non-contact method of surface feature measurement. These general samples consist of a small block of Aluminum alloy with a specific radius cut along one edge. The samples include radii ranging from 0.005” to 0.035” and are shown in Fig. 29.

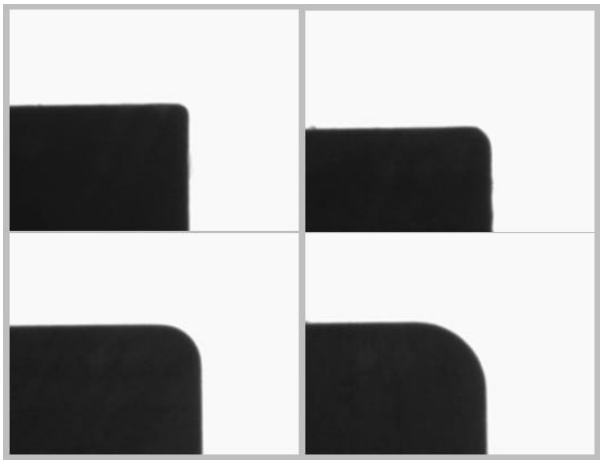

Figure 29. Edge Radii: 0.005", 0.010", 0.020", 0.035"

Results for Contour Measurement Experiments

Once results were obtained through the opto-mechanical method outlined above, measured radius values were compared against known values. Known values were obtained through standard techniques of measurement: the diameters of large cylindrical samples were measured with a caliper and the industry samples were measured independently in a metrology laboratory.

Three large diameter rods were measured using the line laser method. Calculations are presented for the largest diameter sample. Coordinates for all data points are input to a data entry and processing program and a series of mathematical operations are performed to obtain a characteristic radius of curvature for the data. A second-order polynomial trend-line fitted through the data points may be expressed in terms of Equation (12):

$$y = -0.056\,x^{2} + 0.947\,x + 0.233 \qquad (12)$$

First and second derivatives of the function are taken with respect to 'x' and the radius of curvature is obtained through Equation (11). This equation is evaluated at an average (RMS) x-value from the data. All calculated data for the largest diameter sample are presented in the following tables:

2^{nd} Order Poly. Trendline	
$y=(a_2*x\hat{}2)+(a_1*x)+a$	
a_2	-0.0558
a_1	0.9472
a	0.2329

Table 1. Line Laser Trend-line Equation

$dy/dx=(b_2*x)+b_1$	
b_2	-0.1115
b_1	0.9472

Table 2. Line Laser Trend-line 1^{st} Derivative

$d^2y/dx^2=c_2$	
c_2	-0.1115

Table 3. Laser Line Trend-line 2nd Derivative

Radius of Curvature	
$R=[1+(dy/dx)^2]^{3/2}/d^2y/dx$	
x (RMS)	9.9133
R	9.3058

Table 4. Laser Line Trend-line Radius of Curvature

R_{Actual} (mm)	$R_{measured}$ (mm)	Error (%)
9.425	9.3058	1.2643

Table 5. Laser Line Result & Error

A radius of 9.306 mm was measured. A percent error of 1.26% exists between the measured value and the actual value of 9.425 mm.

A table containing all measured radii, known values, and percent error data for the three samples is presented below:

Sample	1	2	3
R_{Actual} (mm)	9.425	6.830	3.985
$R_{Measured}$ (mm)	9.306	5.903	3.833
Error (%)	*1.26*	*13.58*	*3.82*

Table 6. Measured & Actual Values, Percent Error

Uncertainty of Acquired Data for Contour Measurement Experiments

Certain characteristics of the line laser used in the experiment introduce error to the data obtained from images of the samples. These characteristics include the thickness of the line laser and any refraction scattering along its inner and outer edges. Misalignment within the test setup will tend to skew the data points obtained from sample images and introduce error into the calculated data. Error associated with measurement calibration (relating number of pixels to unit length) will propagate through all data and calculations.

Camera resolution has significant influence over data accuracy as this dictates the resolution with which measurements may be made. The influence of this error source over result accuracy increases significantly as the size of the features to be measured decreases and becomes a limiting factor in the measurement accuracy of small radii. It is shown that, with the equipment used in the experiments presented herein, the smallest radius measured with acceptable accuracy has a value of 0.889mm and the measured value has an associated error of 0.29%. Measurement error increases significantly at smaller radii: 77.39% at 0.254mm and 83.70% at 0.127mm.

Camera resolution affects feature edge image clarity and determines the maximum number of data points that may be mapped along a feature of interest. Each of these characteristics is constrained by the relationship of image pixel size to feature geometry dimensions. These parameters must be balanced if accurate results are to be obtained: camera resolution must be sufficient to provide a dense matrix of pixels across a region of interest of an image of a part to be measured. This dense matrix ensures that data points may be mapped across the edge of a part (or line laser

projection) with fine precision and that a large number of data points may be mapped across a given contour, thereby increasing the accuracy with which a trend-line may be fitted to the data set. Machined parts with fine or intricate contours will require that images be taken using a high resolution camera, while large parts with coarse surface geometry may be evaluated using a camera of lower image resolution.

A certain amount of error exists within the process of mapping data points across the feature to be measured. This error is largely associated with the clarity of the image being measured and the resolution of the camera used to capture an image of the sample. Additionally, the precision with which a trend-line may be fitted to a given data set effects measurement accuracy. This is driven by camera resolution and the precision of the data set used to produce the trend-line equation.

Educational Value as Graduate Thesis Topic

The topic discussed in this paper can be used as a Masters Thesis project for Electrical, Mechanical and Computer Engineering students. One of the major challenges of this methodology is the process for software design, implementation, and testing. Basically there are two teaching approaches; (1) focus on the embedded software programming and embedded hardware aspects which include language, computer architecture, and development tools or (2) focus on visual language-neutral programming applications, such as Simulink, MATLAB, Labview, VisSim, and others, which generate less efficient software but do not require the time needed to gain an intimate knowledge of a language and its development environment. It is the author's belief that embedded software development cannot and should not be a focus area for mechanical engineers.

Conclusion

Each of the methods investigated are able to produce results with high accuracy and precision. As the system is designed to be a prototype and for developing the methodology, all parts were selected to be compatible. With a dedicated casing for the elements, a smaller unit can be produced. Measurement accuracy may be increased for both methods through the production of custom fixtures for specific samples. This would allow the relative position of the camera, sample and light source to be fixed, and significantly reducing error associated with misalignment between the camera, sample, and light source. Furthermore, part-specific fixturing would enable processes automation for industrial applications. Specific stations may be produced for each part to be measured and equipment may be selected based on the geometry to be measured. Measurement calibration and lighting conditions may be controlled for each case, further reducing error. The process of mapping control points across the feature to be measured, determining a best-fit equation for the data set and evaluating the radius of curvature for the equation may be automated through software. The entire process may be automated to a point where surface feature assessment may be performed on-line, providing immediate feedback on the pass / no-pass condition of components being assessed.

References

[1] Pheatt, C., Ballester, J., and Wilhelmi D., 2005, "Low-Cost Three-Dimensional Scanning Using Range Imaging," Journal of Computing Sciences in Colleges, 20(4), pp.13-19.
[2] Scott W. R., Roth G., and Rivest J. F., 2003, "View Planning for Automated Three-Dimensional Object Reconstruction and Inspection," ACM Computing Surveys (CSUR), 35(1), pp.64-96.
[3] Fujisawa, S.H., Yokohama, T.O., Yokohama, M.A., and Yokohama, T.O., 1988, "Three-Dimensional Vision System," United States Patent, Patent Number 4,731,853.
[4] Horn, J.N., 1990, "Contour Measurement using Time-based Triangulation Methods," United States Patent, Patent Number 4,939,379.
[5] Vaught, J.L., Fein, M.E., and Neukermans, A.P., 1993, "Speckle Reduction Track Filter Apparatus for Optical Inspection of Patterned Substrates," United States Patent, Patent Number 5,264,912.

[6] Wick, W.R.W., and Wood, P.G., 1997, "Non-Contact Precision Measurement System," United States Patent, Patent Number 5,617,645.
[7] Rockseisen, A., 2000, "Method for the Contact-Free Measurement of the Distance of an Object according to the Principle of Laser Triangulation," United States Patent, Patent Number 6,088,106.
[8]Shetty, Devdas, Ali, Ahad and Hill, Jonathan. "Optomechanical Instrumentation for Vibration Measurement" International Journal of Precision Engineering and Manufacturing Vol. 12, No. 3, pp. 405-411
[9]Shetty, Devdas and Kolk, Ric "Mechatronics System Design" Cengage Learning International, Toronto, 2011

Appendix

Estimation of Error

Determination of the this parameter corresponds to the quantity of the measurement accuracy. As it can be seen from the shapes of the images, obtained experimentally, the measurement error of that geometrical parameter of the testing samples depends on the *x* and *y* coordinates of the given image. The error of measurement of the radius of curvature theoretically can be found from the Equation (1) as:

$$dR \approx \left(\frac{dR}{dx} \right) \cdot dx \tag{13}$$

However upon changing the *x* coordinate value, random values of the *y* coordinate are obtained so that this circumstance makes it impossible to obtain the purely theoretical dependence $R = F_1(x)$. On the other hand the radius of curvature can be found as the function $R = F_2(y)$, because changes in *y* brings changes in the values of *x*. Therefore Equation (13) can be expressed as:

$$dR \approx \left[\frac{dF_1(x)}{dx} \right] \cdot dx \approx \left[\frac{dF_2(y)}{dy} \right] \cdot dy \tag{14}$$

On the basis of these circumstances errors in the measurements of the radius of curvature should be found indirectly. Below is the indirect method for finding different errors of the measurement. The absolute and the relative value of the measurement errors for the given value of the ***x*** can be found on the basis of Fig. 30. They have the forms (Equation (15)):

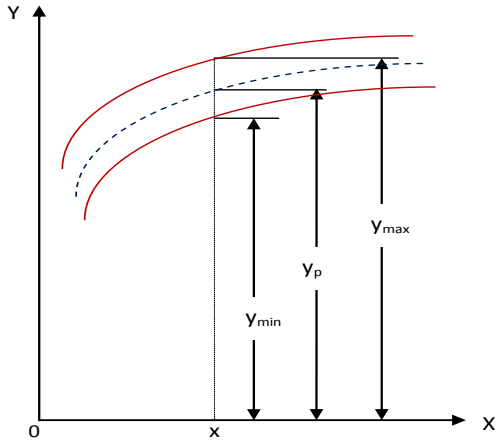

Figure 30. Graphical representation of image used for determination of absolute and relative errors

$$\delta_{abs.} = (y_{\max.} - y_{\min.})$$

$$\delta_{rel.} = \frac{(y_{\max.} - y_{\min.})}{y_p} \tag{15}$$

where $y_{\max}$ and $y_{\min}$ are the maximum and minimum values of the y coordinate of the image representing the upper border **(max.)** and the lower border **(min.)** of the given image (Fig. 24, 27). Consequently y_p represents the polynomial function. Polynomial functions y_p (Equation (12)) can be obtained easily on the basis of the Labview program.

In the range from $x = x_1$ to $x = x_2$ the integral error of the measurement is determined, which is the ratio of the area of the image strip located along the arc (represented by the polynomial function y_p) and the area located between the curve y_p and *x* axis (Fig. 31)

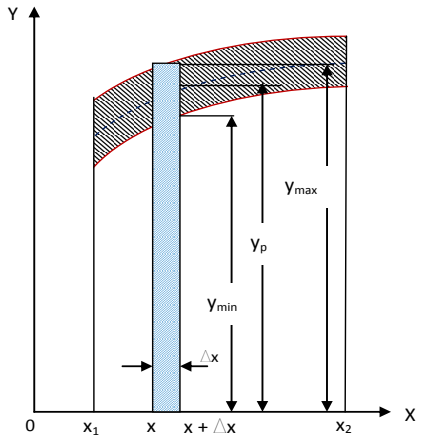

Figure 31. Determination of areas used for estimation of integral error.

$$\delta_{\text{int.}} = \frac{\int_{x_1}^{x_2} (y_{\max} - y_{\min}) \cdot dx}{\int_{x_1}^{x_2} y_p \cdot dx} = \frac{\sum_{x=x_1}^{x=x_2} \sum_{j=1}^{j=n} \delta_{j.abs.} \cdot \Delta x_j}{\int_{x=x_1}^{x=x_2} y_p \cdot dx} \tag{16}$$

where n is the number of division of the interval $(x_2 - x_1)$. .